White-light optical implementation of the fractional Fourier transform with adjustable order control

Enrique Tajahuerce, Genaro Saavedra, Walter D. Furlan, Enrique E. Sicre, and Pedro Andrés

An optical implementation of the fractional Fourier transform (FRT) with broadband illumination is proposed by use of a single imaging element, namely, a blazed diffractive lens. The setup displays an achromatized version of the FRT of order P of any two-dimensional input function. This fractional order can be tuned continuously by shifting of the input along the optical axis. Our compact and flexible configuration is tested with a chirplike input signal, and the good experimental results obtained support the theory. © 2000 Optical Society of America

OCIS codes: 070.6020, 100.0100, 050.1940, 070.2580.

1. Introduction

In spite of its recent introduction in optics, the fractional Fourier transform (FRT) has become an extensively used tool.[1] Among other possibilities, it has been applied to describe the light propagation through optical systems[2–4] and to characterize light beams,[5] and, in particular, its space-variant character has been exploited in several optical information-processing applications.[6–9]

Aside from the original gradient-index-lens device,[1] several optical implementations of the FRT with fixed order have been proposed with use of one or two lenses.[10,11] In these systems the design parameters are determined by the fractional order P to be achieved, and, consequently, this order cannot be modified unless either more lenses are added to the setup[12] or several basic modules are cascaded.[13]

Recently, a lensless configuration for obtaining the FRT of any arbitrary order was reported,[14] in which the fractional order can be varied continuously by a simple shift of the input and the output planes along the optical axis. In Ref. 14 it is also recognized for what is believed to be the first time that, aside from a phase factor and maybe a scaling error, all the FRT's of a given input function can be obtained simultaneously, dispersed along the optical axis, by free-space propagation of the electromagnetic field. This variable-order capability has been successfully applied to image processing[15] and to the optical production of some phase-space representations of signals.[16]

One of the main drawbacks of the above optical implementations is the use of monochromatic coherent illumination, which leads, in general, to a poor signal-to-noise ratio. Moreover, when used in optical processing, their application is restricted to gray-scale images. Therefore there is a strong practical motivation to design an optical setup for overcoming these limitations by use of broadband illumination.

In this paper we present an optical implementation of the FRT of a two-dimensional signal, using a white-light point source. The setup contains a single optical element, namely, a blazed diffractive lens (DL). The proposed device provides an achromatized version of the FRT of order P of the input signal along the lines of what is discussed in Refs. 17 and 18. In this way it is able to superimpose, to a first-order approximation, all the monochromatic versions of the FRT of order P generated by the different spectral components of the incident light in a single plane and with the same magnification. This new, to our knowledge, optical proposal shows an adjustable fractional-order control, as in Ref. 14, such that the order of the achromatic FRT can be continuously tuned by appropriate shifting of the input and the output planes along the optical axis. For the sake of completeness

E. Tajahuerce is with the Departamento de Ciencias Experimentales, Universitat Jaume I, E-12080 Castelló, Spain. G. Saavedra, W. D. Furlan, and P. Andrés (pedro.andres@uv.es) are with the Departamento de Óptica, Universitat de València, E-46100 Burjassot, Spain. E. E. Sicre is with the Centro de Investigaciones Ópticas, Casilla de Correo 124, 1900 La Plata, Argentina.

Received 28 May 1999; revised manuscript received 21 October 1999.

0003-6935/00/020238-08$15.00/0

the basic relationships between fractional Fourier transformation and propagation in free space are reviewed in Section 2. In Section 3 we present the theoretical basis of our compact white-light order-tunable FRT device, and in Section 4 we show some experimental results for a chirplike test signal.

2. Coherent Free-Space Fractional-Fourier-Transform Implementation

The FRT of a given two-dimensional function $g(\boldsymbol{\rho})$ is defined as[19,20]

$$G_P(\mathbf{w}) = \frac{i\exp(i\phi)}{\sin\phi}\exp\left(\frac{i\pi|\mathbf{w}|^2}{\tan\phi}\right)\iint_{-\infty}^{+\infty} g(\boldsymbol{\rho}) \times \exp\left(\frac{i\pi|\boldsymbol{\rho}|^2}{\tan\phi}\right)\exp\left(-\frac{i2\pi\boldsymbol{\rho}\cdot\mathbf{w}}{\sin\phi}\right)\mathrm{d}^2\boldsymbol{\rho}, \quad (1)$$

where $\phi = P\pi/2$, P being the order of the FRT. Note that the FRT is a periodic function in terms of P, with period 4. In addition, since $G_{P+2}(\mathbf{w}) = G_P(-\mathbf{w})$, the whole information about the FRT of any order can be obtained by consideration of only values of P ranging in the interval (0, 2). The FRT turns out the conventional Fourier transformation for $P = 1$, whereas $P = 2$ provides an inverted replica of the object, $g(-\boldsymbol{\rho})$.

It is well known that there is a close relationship between the FRT and the Fresnel diffraction integral. As was pointed out in Refs. 14 and 21, every Fresnel diffraction pattern of a transparency illuminated with a monochromatic point source corresponds to a scaled version of a certain FRT of the same input, and vice versa. To establish this connection in mathematical terms, let us assume that a monochromatic spherical wave front illuminates an input object, as is illustrated in Fig. 1. The field amplitude across a transversal plane at a distance R from the diffracting screen is given, within the Fresnel approximation, by

$$U_R(\mathbf{r};\lambda,z) = \frac{i}{\lambda R}\exp\left(\frac{i\pi}{\lambda R}|\mathbf{r}|^2\right)\iint_{-\infty}^{+\infty} t(\mathbf{r}_0) \times \exp\left(\frac{i\pi}{\lambda}\frac{z+R}{zR}|\mathbf{r}_0|^2\right) \times \exp\left(-\frac{i2\pi\mathbf{r}_0\cdot\mathbf{r}}{\lambda R}\right)\mathrm{d}^2\mathbf{r}_0, \quad (2)$$

where $t(\mathbf{r}_0)$ represents the two-dimensional complex amplitude transmittance of the object, λ is the wavelength of the illuminating wave front, and z is the distance from the focus of the illumination field to the object plane. Note that $z < 0$ when a spherical converging beam acts as incident illumination. As is usual in the optical implementation of mathematical transformations, we introduce the dimensionless variables

$$\boldsymbol{\rho} = (\mathbf{r}_0/s), \qquad \mathbf{w} = (\mathbf{r}/s), \quad (3)$$

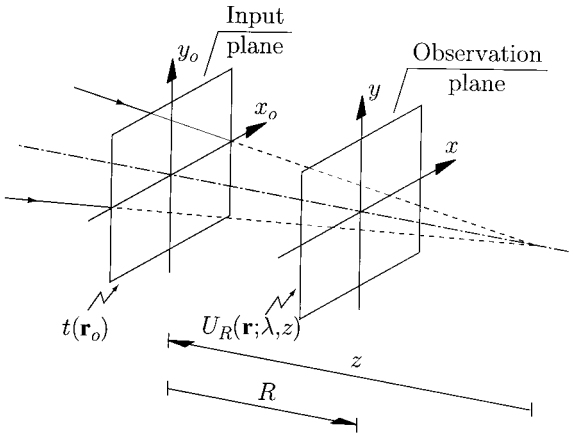

Fig. 1. Free-space FRT setup.

where s is a scale parameter. In this way Eq. (2) can be rewritten as

$$\hat{U}_R(\mathbf{w};\lambda,z) = \frac{is^2}{\lambda R}\exp\left(\frac{i\pi s^2}{\lambda R}|\mathbf{w}|^2\right)\iint_{-\infty}^{+\infty} g(\boldsymbol{\rho}) \times \exp\left(\frac{i\pi}{\lambda}\frac{z+R}{zR}s^2|\boldsymbol{\rho}|^2\right) \times \exp\left(-\frac{i2\pi s^2\boldsymbol{\rho}\cdot\mathbf{w}}{\lambda R}\right)\mathrm{d}^2\boldsymbol{\rho}, \quad (4)$$

being $\hat{U}_R(\mathbf{w};\lambda,z) = U_R(\mathbf{r};\lambda,z)$ and $g(\boldsymbol{\rho}) = t(\mathbf{r}_0)$. When we compare Eqs. (1) and (4), aside from the quadratic phase factors that precede both integrals, the mathematical relationship between the FRT of order P of the signal $g(\boldsymbol{\rho})$ and the Fresnel diffraction field generated by the input amplitude transmittance $t(\mathbf{r}_0) = g(\mathbf{r}_0/s)$, under spherical illumination, can be expressed as[14]

$$\hat{U}_R(\mathbf{w};\lambda,z) \propto G_P\left[\frac{\mathbf{w}}{M(P;\lambda,z)}\right]. \quad (5)$$

The FRT is obtained at a distance

$$R(P;\lambda,z) = \frac{f(\lambda)\tan(P\pi/2)}{1-[f(\lambda)/z]\tan(P\pi/2)} \quad (6)$$

from the input plane, and the scale factor error is

$$M(P;\lambda,z) = \frac{1}{\{1-[f(\lambda)/z]\tan(P\pi/2)\}\cos(P\pi/2)}. \quad (7)$$

In Eqs. (6) and (7), $f(\lambda) = s^2/\lambda$. We recognize that this parameter is simply the standard focal length used in many FRT-related papers.

It is important to note that by use of this simple configuration the FRT's of all orders of the input are obtained simultaneously by free-space propagation. In addition, a proper selection of the distance z allows one to obtain a specific FRT without scale error. However, from a practical point of view, this setup shares all the drawbacks associated with coherent

optical processors. To overcome them, in Section 3 we present a white-light optical implementation of the FRT.

3. Achromatic Fractional Fourier Transformer

The use of the setup in Fig. 1 for producing a polychromatic optical implementation of the FRT fails because of the dependence of both the distance $R(P; \lambda, z)$ and the magnification $M(P; \lambda, z)$ on the wavelength. In this way the monochromatic versions of the FRT with a fixed fractional order P are chromatically dispersed along the optical axis and show a different magnification in each chromatic channel. Since the output plane contains the incoherent superposition of all spectral components, this fact results in a chromatic blur of the output FRT.

To quantify this chromatic blurring, let us choose as the output plane that in which the FRT of order P of the input signal is obtained for a typical wavelength λ_0. According to Eq. (6), over the same plane we achieve, for each wavelength λ, the FRT of a different order, $Q(\lambda, P)$, such that

$$R(Q; \lambda, z) = R(P; \lambda_0, z). \tag{8}$$

In addition, the magnification error in each chromatic component is given, according to Eq. (7), by $M(Q; \lambda, z)$.

To evaluate the above chromatic deviations in each chromatic channel, we introduce the relative errors

$$\Delta Q(\lambda, P) = \frac{Q(\lambda, P) - P}{P}, \tag{9}$$

$$\Delta M(\lambda, P) = \frac{M[Q(\lambda, P); \lambda, z] - M(P; \lambda_0, z)}{M(P; \lambda_0, z)}. \tag{10}$$

By use of Eqs. (6)–(8), these error functions can be expressed as

$$\Delta Q(\lambda, P) = \frac{2}{P\pi} \arctan\left[\frac{\lambda}{\lambda_0} \tan(P\pi/2)\right] - 1, \tag{11}$$

$$\Delta M(\lambda, P) = \left[\frac{1 + (\lambda/\lambda_0)^2 \tan^2(P\pi/2)}{1 + \tan^2(P\pi/2)}\right]^{1/2} - 1. \tag{12}$$

A plot of these relative errors versus the wavelength λ, for both the fractional order and the magnification, is shown in Figs. 2(a) and 2(b), respectively, for different values of the selected order P. In this figure we assume that λ_0 lies in the middle of the visible region and that the spectral content of the incident light covers the whole visible spectrum. We note that chromatic errors to as great as $\pm 40\%$ are achieved in the extremes of the visible region for certain fractional orders P, these values being unacceptable in practice.

To overcome this drawback, let us modify the optical setup in Fig. 1 by introducing a blazed DL on the transversal plane containing the real focus of the incident broadband spherical wave front, as is depicted in Fig. 3. The DL acts as an optical imaging

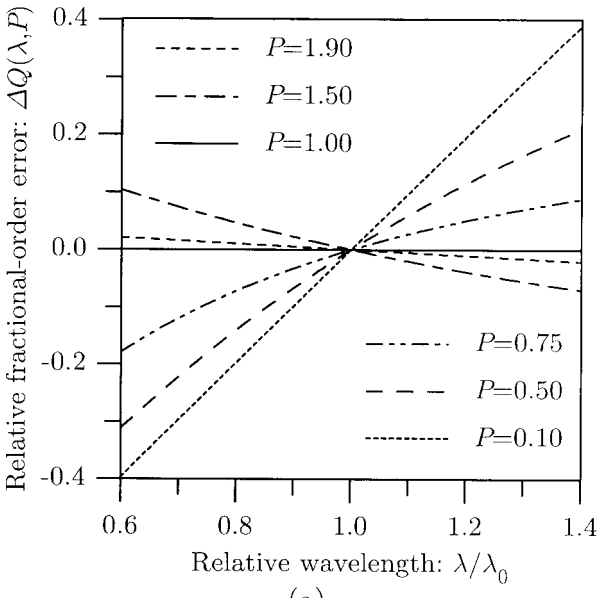

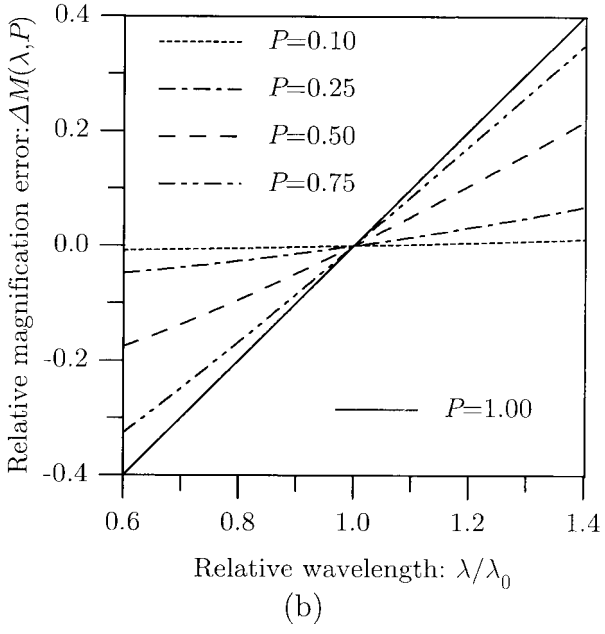

Fig. 2. Relative chromatic errors obtained when broadband illumination is used in the setup shown in Fig. 1: (a) fractional-order error, (b) magnification error. Note that only values $P \in (0, 1)$ are represented in (b), since the same curves are obtained by exchange of P by $2 - P$. In both plots we choose $\lambda_0 = 600$ nm.

element with a focal length $Z(\lambda)$ that is proportional to λ^{-1}, namely, $Z(\lambda) = Z_0\lambda_0/\lambda$. The constant Z_0 is simply the value of the focal length for the reference wavelength λ_0. In this way, within the paraxial approximation, a DL is characterized by an amplitude transmittance

$$D(\mathbf{r}) = \exp\left(-\frac{i\pi|\mathbf{r}|^2}{\lambda_0 Z_0}\right). \tag{13}$$

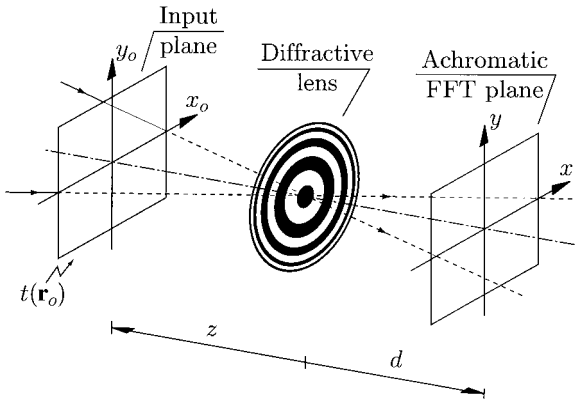

Fig. 3. White-light fractional Fourier transformer.

It is straightforward to show that the diffraction pattern obtained at a distance d from the DL is given, aside from some constants and phase factors, by

$$U'_d(\mathbf{r};\lambda,z,Z_0)=\iint_{-\infty}^{+\infty}t(\mathbf{r}_0)\exp\left(-\frac{i\pi|\mathbf{r}_0|^2}{\lambda\alpha z}\right)\times\exp\left(\frac{i2\pi\mathbf{r}_0\cdot\mathbf{r}}{\lambda\alpha d}\right)\mathrm{d}^2\mathbf{r}_0, \tag{14}$$

where

$$\alpha=z\left(\frac{1}{d}-\frac{1}{z}-\frac{\lambda}{\lambda_0 Z_0}\right). \tag{15}$$

By performing the change of variables indicated in Eq. (3), we obtain

$$\hat{U}'_d(\mathbf{w};\lambda,z,Z_0)=\iint_{-\infty}^{+\infty}g(\boldsymbol{\rho})\exp\left(-\frac{i\pi s^2|\boldsymbol{\rho}|^2}{\lambda\alpha z}\right)\times\exp\left(\frac{i2\pi s^2\boldsymbol{\rho}\cdot\mathbf{w}}{\lambda\alpha d}\right)\mathrm{d}^2\boldsymbol{\rho}, \tag{16}$$

where $\hat{U}'_d(\mathbf{w};\lambda,z,Z_0)=U'_d(\mathbf{r};\lambda,z,Z_0)$. Finally, by comparing this result with definition (1), we have

$$\hat{U}'_d(\mathbf{w};\lambda,z,Z_0)\propto G_P\left[\frac{\mathbf{w}}{M'(P;\lambda,z,Z_0)}\right], \tag{17}$$

if we select the distance d as

$$d(P;\lambda,z,Z_0)=\frac{zZ_0}{Z_0+z\dfrac{\lambda}{\lambda_0}-\dfrac{Z_0 f(\lambda)}{z}\tan(P\pi/2)}. \tag{18}$$

Here the scale factor error is

$$M'(P;\lambda,z,Z_0)=\frac{d(P;\lambda,z,Z_0)}{z\cos(P\pi/2)}. \tag{19}$$

Equations (18) and (19) state that the FRT of fractional order P is still chromatically dispersed both in longitudinal position and in transversal magnification. However, unlike the setup in Fig. 1 [see Eqs. (6) and (7)], now it is possible to partially compensate both chromatic errors by a proper selection of the geometrical parameters of the setup.

To this end we pay attention to the plane in which the FRT of order P for the reference wavelength λ_0 is located. Over this plane each wavelength λ provides a FRT of order $Q'(\lambda,P,z,Z_0)$, where Q' is the solution of the equation

$$d(Q';\lambda,z,Z_0)=d(P;\lambda_0,z,Z_0); \tag{20}$$

i.e., according to Eq. (18),

$$\tan(Q'\pi/2)=\left(\frac{\lambda}{\lambda_0}-1\right)\frac{\lambda}{\lambda_0}\frac{z^2}{f(\lambda_0)Z_0}+\frac{\lambda}{\lambda_0}\tan(P\pi/2). \tag{21}$$

Moreover, each FRT of order Q' is affected by a different scaling error given by

$$M'(Q';\lambda,z,Z_0)=\frac{d(P;\lambda_0,z,Z_0)}{z\cos(Q'\pi/2)}=M'(P;\lambda_0,z,Z_0)\times\left[\frac{1+\tan^2(Q'\pi/2)}{1+\tan^2(P\pi/2)}\right]^{1/2}. \tag{22}$$

The design of our setup is carried out by imposition of an achromatic behavior around the reference wavelength λ_0 at the output plane to both the fractional order and the magnification factor. This approach guarantees that both functions present stationary values in the vicinity of $\lambda=\lambda_0$. In mathematical terms we require

$$\frac{\mathrm{d}}{\mathrm{d}\lambda}Q'(\lambda,P,z,Z_0)\bigg|_{\lambda_0}=0, \tag{23}$$

$$\frac{\mathrm{d}}{\mathrm{d}\lambda}M'(Q';\lambda,z,Z_0)\bigg|_{\lambda_0}=0. \tag{24}$$

From Eq. (22) it is apparent that M' depends on λ only through the quantity Q'. Therefore Eqs. (23) and (24) lead to the same requirement. Combining Eqs. (21) and (23), we obtain

$$z^2=-Z_0 f(\lambda_0)\tan(P\pi/2). \tag{25}$$

This result provides the value of the distance z from the DL to the input transparency that has to be selected to achieve an achromatized version of the FRT of order P of the input signal. It is worth mentioning that Eq. (25) also imposes the prescription for the convergence or divergence of the DL employed in the design, since a real solution for the distance z is obtained only when $Z_0\tan(P\pi/2)<0$. Note also that only solutions with $z<0$ are physically acceptable in the proposed setup, as can be seen in Fig. 3.

To complete the analysis of our proposal, we test the performance of the optimized device by obtaining the residual chromatic errors at the output plane.

The substitution of the constraint (25) into Eqs. (21) and (22) leads to

$$\tan(Q'\pi/2) = \{1 - [(\lambda/\lambda_0) - 1]^2\}\tan(P\pi/2), \quad (26)$$

$$M'(Q'; \lambda, z, Z_0) = M'(P; \lambda_0, z, Z_0) \times \left(\frac{1 + \{1 - [(\lambda/\lambda_0) - 1]^2\}^2 \tan^2(P\pi/2)}{1 + \tan^2(P\pi/2)}\right)^{1/2}. \quad (27)$$

In the previous equation the parameter

$$M'(P; \lambda_0, z, Z_0) = \frac{d(P; \lambda_0, z, Z_0)}{z}[1 + \tan^2(P\pi/2)]^{1/2} \quad (28)$$

is the scale factor of the P-order FRT obtained for $\lambda = \lambda_0$, being

$$d(P; \lambda_0, z, Z_0) = \frac{z^2}{z - 2f(\lambda_0)\tan(P\pi/2)} \quad (29)$$

the distance from the DL to the output plane.

For characterizing these residual chromatic aberrations over the output plane, we calculate the relative error in the fractional order for each chromatic channel through the function

$$\Delta Q'(\lambda, P) = \frac{Q'(\lambda, P, z, Z_0) - P}{P} = \frac{2}{P\pi}\arctan(\{1 - [(\lambda/\lambda_0) - 1]^2\} \times \tan(P\pi/2)) - 1. \quad (30)$$

The relative error in the magnification factor is calculated in a similar way by means of the parameter

$$\Delta M'(\lambda, P) = \frac{M'[Q'(\lambda, P, z, Z_0); \lambda, z, Z_0] - M'(P; \lambda_0, z, Z_0)}{M'(P; \lambda_0, z, Z_0)} = \left(\frac{1 + \{1 - [(\lambda/\lambda_0) - 1]^2\}^2 \tan^2(P\pi/2)}{1 + \tan^2(P\pi/2)}\right)^{1/2} - 1. \quad (31)$$

A graphical representation of these merit functions, associated to each chromatic channel, is presented in Fig. 4 for different values of the selected order P. The typical achromatic behavior is clearly shown in this picture, and it is remarkable that a sensible reduction of the fractional errors is achieved compared with the free-space FRT device in Fig. 2.

In summary, given a DL—characterized by its focal length Z_0—and an overall scale factor s for the input transparency, Eq. (25) provides the appropriate distance z between the input transparency and the DL for achieving an achromatized version of the FRT of any fractional order P. In this situation the achromatic FRT is obtained over a plane located at a distance $d(P; \lambda_0, z, Z_0)$ from the DL and scaled by a factor $M'(P; \lambda_0, z, Z_0)$ given in Eqs. (29) and (28), respectively. Note that positive and negative values of the distance $d(P; \lambda_0, z, Z_0)$ correspond to real and virtual output planes, respectively. Although real output planes are usually preferred for direct observation, the use of a simple telecentric achromatic optical system allows one to deal with virtual planes as well.

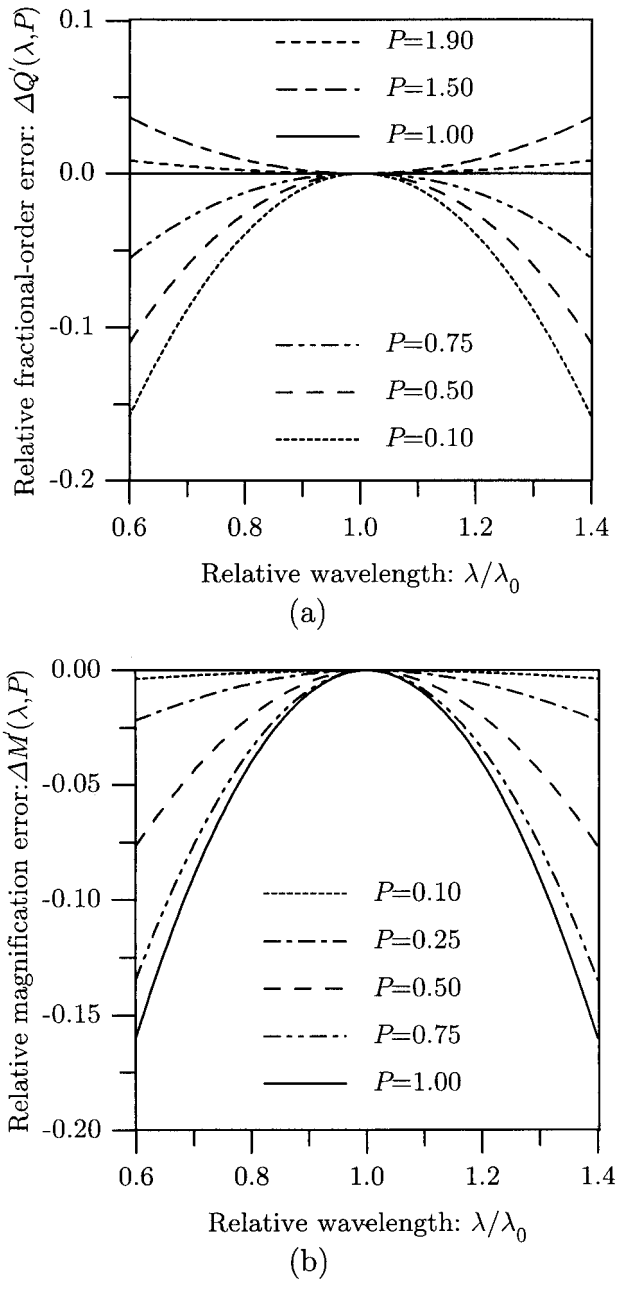

Fig. 4. Fractional errors affecting each chromatic channel in the optimal design of the setup presented in Fig. 3: (a) fractional-order error, (b) magnification error. As in Fig. 2, only values $P \in (0, 1)$ are considered for the magnification error because of the invariance of this function under the change of P by $2 - P$. We also choose here $\lambda_0 = 600$ nm.

Finally, it is worth mentioning that the design parameters of the system, namely, the focal length Z_0 and the construction scale factor s of the input transparency, can be properly chosen to provide a unity

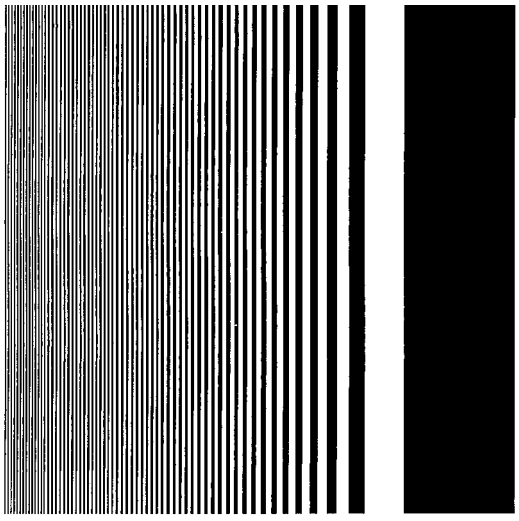

Fig. 5. Input function consisting of a binary grating with linearly increasing spatial frequency (chirplike function).

magnification for a fixed desired fractional order, as can be deduced from Eqs. (25), (28), and (29).

In Section 4 we present an experimental verification of the proposed achromatic fractional Fourier transformer, and we discuss the performance of the optical system.

4. Experimental Results

Although our proposal can work with any two-dimensional signal, in the experimental verification we choose as input object a conventional one-dimensional FRT test, namely, a linear encoding of a real one-dimensional chirplike signal. Thus we use a binary grating whose spatial frequency is linearly variable, as is shown in Fig. 5. This object presents an amplitude transmittance that codifies, basically, the function

$$g(\boldsymbol{\rho}) = \begin{cases} \sum_{n=0}^{\infty} g_n \cos(\pi n \alpha \rho_x^2), & \text{if } -L < \rho_x \le 0 \\ 0, & \text{otherwise} \end{cases}, \quad (32)$$

α being the so-called chirp rate of the signal, ρ_x the coordinate in the direction of variation of the one-dimensional signal, L the finite extent of the object in this direction, and g_n a set of real coefficients. It is straightforward to show that this class of functions presents some characteristic FRT's that are highly localized around a narrow focusing line. The focusing fractional orders satisfy the relation

$$\tan(P_{\pm n}\pi/2) = \pm 1/(n\alpha) \qquad \text{for all } n \neq 0/g_n \neq 0. \quad (33)$$

In our experiment we generated the input transparency by coding a binary one-dimensional chirplike signal with chirp rate $\alpha = 4$. We fixed our attention in the fractional order P_{-1}, which, according to Eq. (33), takes the value $P = P_{-1} = 1.844$. The overall scale factor for the encoding of the signal onto the amplitude transmittance of the input object was $s = 1$ mm.

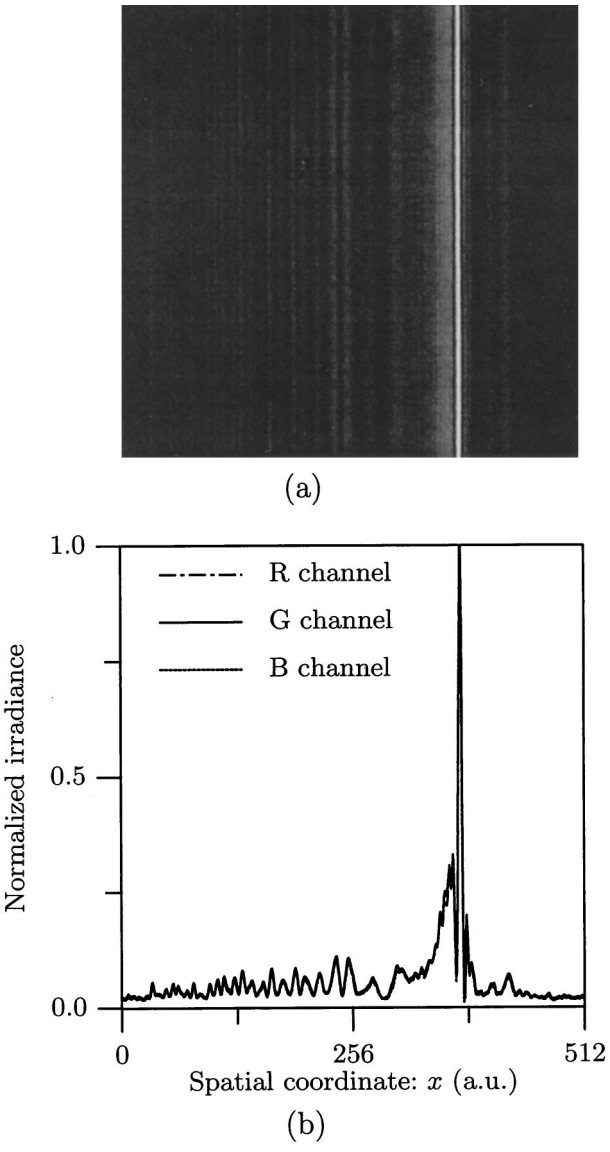

Fig. 6. Achromatic FRT obtained by use of the setup in Fig. 3 under white-light illumination: (a) gray-scale display of the irradiance, (b) profile of the irradiance along the horizontal direction for each RGB component of the registered image.

For implementing the achromatic setup in Fig. 3 we used a DL with focal length $Z_0 = 94.2$ mm for a reference wavelength $\lambda_0 = 546.1$ mm. This DL was a four-level diffractive element constructed with multimask-level technology in photoresist and beam etched over synthetic fused silica. The diffraction efficiency for the principal focal length is limited to approximately 70%.

As was mentioned above, the proper choice of the distance z from the DL to the input transparency allows us to select the fractional order P of the output achromatic FRT. For the fractional order of our interest, we chose a value of $z = -207.66$ mm, according to Eq. (25). In this way the achromatic output

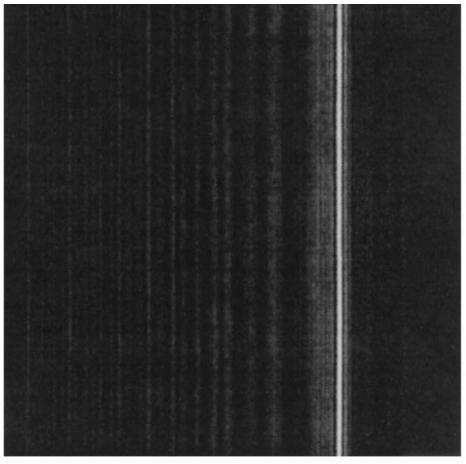

(a)

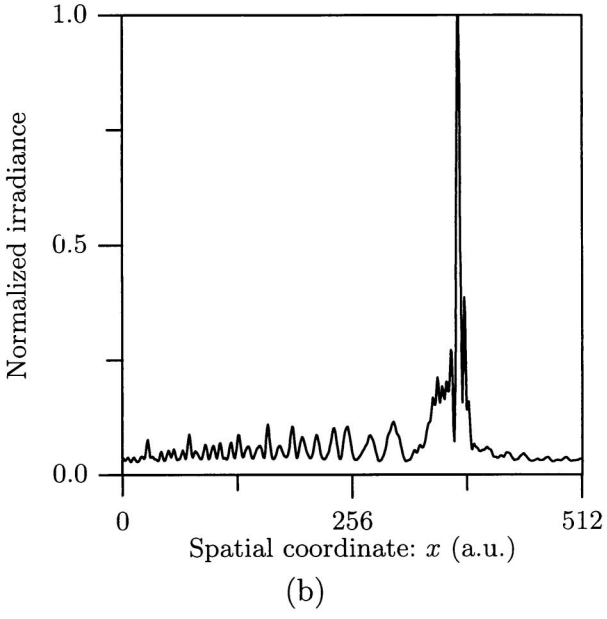

(b)

Fig. 7. Monochromatic FRT obtained by the free-space propagation setup in Fig. 1: (a) gray-scale register of the irradiance, (b) horizontal profile of the image in (a).

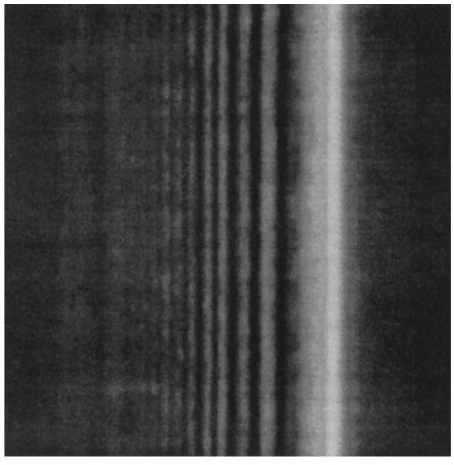

(a)

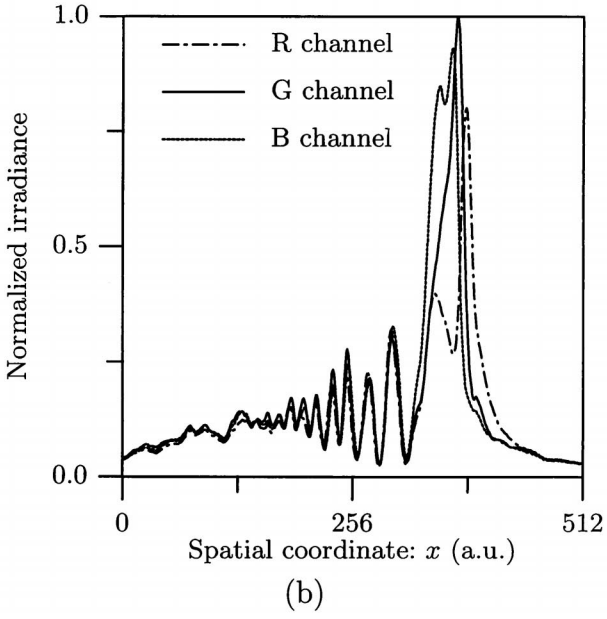

(b)

Fig. 8. Same as in Fig. 7 but obtained with polychromatic illumination: (a) gray-scale display of the irradiance, (b) horizontal profile of each RGB component of the registered image.

plane was located at a distance $d = 60.91$ mm from the DL, as can be obtained from Eq. (29).

The input object was illuminated with a polychromatic spherical wave front obtained from a high-pressure mercury arc lamp, and the irradiance distribution at the output plane was registered by use of a color CCD camera. A gray-scale picture of the result is presented in Fig. 6(a). The graph in Fig. 6(b) shows the profiles of the irradiance distribution along a horizontal line corresponding to the red–green–blue (RGB) chromatic components of the CCD.

To appreciate the correction of the chromatic blurring obtained at the output plane of our achromatic system, we present in Figs. 7 and 8 the results provided by the conventional noncorrected optical system in Fig. 1 for the same input object. Figure 7(a) shows a picture of the irradiance distribution corresponding to the previous FRT when monochromatic illumination with $\lambda = \lambda_0$ is used. In Fig. 7(b) we show the irradiance profile along the horizontal direction in Fig. 7(a). The irradiance pattern obtained at the same observation plane when the object is illuminated by the polychromatic radiation arising from the mercury lamp is shown as a gray-scale picture in Fig. 8(a). The irradiance profiles corresponding to the RGB chromatic components of this register are presented in Fig. 8(b). From this picture the chromatic blurring produced by the diffraction phenomenon can be clearly seen. The comparison between Figs. 6(b), 7(b), and 8(b) shows that the first result is almost unaffected by chromatic blurring, confirming the good performance of the proposal.

5. Conclusions

We have presented and experimentally verified a simple design of a fractional Fourier transformer that operates with polychromatic illumination. The system allows for a continuous range of values of the FRT fractional order P at the output plane by appropriate shifting of the input and the output planes. The optical configuration uses only a single commercially available diffractive optical element, namely, a kinoform DL. The system has been implemented, and the experimental results obtained support the theory. Our proposal can be considered to be the first stage of a FRT processor working with white light, with potential applications in space-variant processing of color signals with a high signal-to-noise ratio.

This study was funded in part through an agreement between the Universitat Jaume I and the Fundacio Caixa Costello (Grant P1B98-14), Spain.

References

1. A. W. Lohmann, D. Mendlovic, and Z. Zalevsky, "Fractional transformations in optics," Prog. Opt. **38,** 265–342 (1998).
2. T. Alieva, V. López, F. Agulló-López, and L. B. Almeida, "The fractional Fourier transform in optical propagation problems," J. Mod. Opt. **41,** 1037–1044 (1994).
3. H. M. Ozaktas and D. Mendlovic, "Fractional Fourier optics," J. Opt. Soc. Am. A **12,** 743–751 (1995).
4. B. Lü, F. Kong, and B. Zhang, "Optical systems expressed in terms of fractional Fourier transforms," Opt. Commun. **137,** 13–16 (1997).
5. D. Dragoman, "Fractional Wigner distribution function," J. Opt. Soc. Am. A **13,** 474–478 (1996).
6. D. Mendlovic, H. M. Ozaktas, and A. W. Lohmann, "Fractional correlation," Appl. Opt. **34,** 303–309 (1995).
7. J. García, D. Mendlovic, Z. Zalevsky, and A. W. Lohmann, "Space-variant simultaneous detection of several objects by the use of multiple anamorphic fractional-Fourier-transform filters," Appl. Opt. **35,** 3945–3952 (1996).
8. S. Granieri, O. Trabocchi, and E. E. Sicre, "Fractional Fourier transform applied to spatial filtering in the Fresnel domain," Opt. Commun. **119,** 275–278 (1995).
9. Z. Zalevsky, D. Mendlovic, and J. H. Caulfield, "Localized, partially space-invariant filtering," Appl. Opt. **36,** 1086–1092 (1997).
10. A. W. Lohmann, "Image rotation, Wigner rotation, and the fractional Fourier transform," J. Opt. Soc. Am. A **10,** 2181–2186 (1993).
11. S. Liu, J. Xu, Y. Zhang, L. Chen, and C. Li, "General optical implementations of fractional Fourier transforms," Opt. Lett. **20,** 1053–1055 (1995).
12. A. W. Lohmann, "A fake zoom lens for fractional Fourier experiments," Opt. Commun. **115,** 437–443 (1995).
13. R. G. Dorsch, "Fractional Fourier transformer of variable order based on a modular lens system," Appl. Opt. **34,** 6016–6020 (1995).
14. P. Andrés, W. D. Furlan, G. Saavedra, and A. W. Lohmann, "Variable fractional Fourier processor: a simple implementation," J. Opt. Soc. Am. A **14,** 853–858 (1997).
15. J. García, R. G. Dorsch, A. W. Lohmann, C. Ferreira, and Z. Zalevsky, "Flexible optical implementation of fractional Fourier transform processors. Applications to correlation and filtering," Opt. Commun. **133,** 393–400 (1997).
16. S. Granieri, W. D. Furlan, G. Saavedra, and P. Andrés, "Radon–Wigner display: a compact optical implementation with a single varifocal lens," Appl. Opt. **36,** 8363–8369 (1997).
17. G. M. Morris and D. A. Zweig, "White-light Fourier transformations," in *Optical Signal Processing*, J. L. Horner, ed. (Academic, San Diego, Calif., 1987), pp. 23–71.
18. J. Lancis, E. Tajahuerce, P. Andrés, V. Climent, and E. Tepichin, "Single-zone-plate achromatic Fresnel-transform setup: pattern tunability," Opt. Commun. **136,** 297–305 (1997).
19. E. U. Condon, "Immersion of the Fourier transform in a continuous group of functional transformations," Proc. Natl. Acad. Sci. USA **23,** 158–164 (1937).
20. V. Namias, "The fractional Fourier transform and its applications to quantum mechanics," J. Inst. Math. Its Appl. **25,** 241–265 (1980).
21. P. Pellat-Finet, "Fresnel diffraction and the fractional-order Fourier transform," Opt. Lett. **19,** 1388–1390 (1994).